

# Interpenetrating Self-Supporting Networks from Anisotropic Semiconductor Nanoparticles and Noble Metal Nanowires

Marina Rosebrock, Jakob Schlenkrich, Hannah Christmann, Rebecca Graf, Patrick Bessel, Dirk Dorfs, Dániel Zámbo, and Nadja C. Bigall\*

In this work, a new type of multicomponent nanostructures is introduced by forming interpenetrating networks of two different nanomaterials. In detail, gel networks from semiconductor nanorods are interpenetrated by Au nanowires. Two different types of gelling agents, namely  $S^{2-}$  and  $Yb^{3+}$ , are employed to trigger the network formation. The structural and electrochemical properties of the resulting materials are discussed. (Photo)electrochemical measurements are performed on the structures to compare the materials in terms of their conductivity as well as their efficiency in converting photonic energy to electrical energy. The new type of CdSe/CdS: Au nanostructure gelled with  $S^{2-}$  shows one order of magnitude higher photocurrent than the system gelled with  $Yb^{3+}$ . Moreover, the introduction of Au nanowires exhibit a photocurrent which is two orders of magnitudes higher than in samples without Au nanowires.

## 1. Introduction

In materials chemistry, nanoparticle assemblies represent an emerging topic that has become increasingly important over the years.<sup>[1–6]</sup> A key advantage is that nanoparticles have manifold properties that differ significantly from those of bulk materials. Among others, examples such as the localized surface plasmon resonance of noble metal nanoparticles<sup>[7]</sup> or the size quantization effect in semiconductor nanoparticles<sup>[8,9]</sup> can be mentioned. Due to their high surface-to-volume ratios, nanoparticles are perfectly suited for processes that take place at the surface.<sup>[10]</sup> This endows them, e.g., with outstanding catalytic activity or sensitivity in sensing applications.<sup>[1,11–20]</sup>

By assembling the individual nanoparticle building blocks to, e.g., self-supporting macroscopic heterostructures, the nanoscopic properties can also be preserved and even extended in larger structural units such as hydrogels and aerogels beside generating new properties. Quasi type II semiconductors such as CdSe/CdS have recently been discussed to ensure transfer of photoexcited electrons to other particles via crystal contact manifesting in an effective charge-carrier separation.<sup>[5,21,22]</sup> If semiconductor nanoparticles are fabricated with bandgaps in the visible spectral region, photoexcited electrons can be generated upon visible-light irradiation within the structure. The combination of semiconductors and noble metals in nanoparticles is particularly suitable for charge-carrier separation, since the electrical contact with the metal effectively supports the accumulation of the electrons which are thus no longer available for radiative recombination processes.<sup>[23]</sup> In a previous work of our group, this type of material combination has already been investigated, in nanocrystal-based gels as well, and the spatially tunable fluorescence quenching as a result of semiconductor–metal contact within a nanoparticle network is investigated.<sup>[22]</sup> Other works known from literature have also used mixed systems of semiconductor and noble metal, which can be called multicomponent or hybrid networks.<sup>[6,24–27]</sup> For example, Hendel et al. showed mixed CdTe and Au spherical nanoparticles<sup>[28]</sup> similar to Nahar et al.<sup>[29]</sup> where spherical CdSe and Ag are combined in a mixed network gelled with tetranitromethane from unpolar solvents. However, in the present work, a combination of CdSe/CdS semiconductor nanorods (NR) with noble metal Au nanowires is used to fabricate an interpenetrating


M. Rosebrock, J. Schlenkrich, H. Christmann, R. Graf, P. Bessel, D. Dorfs, N. C. Bigall

Institute of Physical Chemistry and Electrochemistry  
Leibniz Universität Hannover  
30167 Hanover, Germany  
E-mail: nadja.bigall@pci.uni-hannover.de

M. Rosebrock, R. Graf, P. Bessel, D. Dorfs, N. C. Bigall  
Laboratory for Nano and Quantum Engineering  
Leibniz Universität Hannover  
30167 Hanover, Germany

M. Rosebrock, D. Dorfs, N. C. Bigall  
Cluster of Excellence PhoenixD (Photonics, Optics and Engineering –  
Innovation Across Disciplines)  
Leibniz Universität Hannover  
30167 Hanover, Germany

D. Zámbo  
Institute of Technical Physics and Materials Science  
Centre for Energy Research  
1121 Budapest, Hungary

 The ORCID identification number(s) for the author(s) of this article can be found under <https://doi.org/10.1002/sstr.202300225>.

© 2023 The Authors. Small Structures published by Wiley-VCH GmbH. This is an open access article under the terms of the Creative Commons Attribution License, which permits use, distribution and reproduction in any medium, provided the original work is properly cited.

DOI: 10.1002/sstr.202300225

semiconductor–metal network. To the best of our knowledge, it is the first interpenetrating gel network consisting of crystalline semiconductor and noble metal components. The morphology of the gold in the shape of nanowires enables the efficient transport of charge carriers. To investigate the effect of the gelling ion, two systems are studied: 1) CdSe/CdS:Au NRs:nanowires gelled with  $S^{2-}$ -ions<sup>[30]</sup>; and 2) CdSe/CdS:Au gelled with  $Yb^{3+}$ -ions, both resulting in two different architectures. We correlate fundamental differences between the different resulting material properties to their structures.

## 2. Results and Discussion

Regarding the semiconductor building blocks, prior to gelation, the NR samples were transferred to water in two different ways leading to either positively or negatively charged samples. CdSe/CdS(–)NRs with 3-mercaptopropionic acid (MPA) ligands have a negative zeta potential in aqueous KOH solution owing to the deprotonation of the carboxyl group of MPA. The negative charge of the ligands attracts  $Yb^{3+}$ -ions toward the surface during gelation, initiating network formation according to Zámbo et al.<sup>[31]</sup> In contrast, CdSe/CdS(+) NRs with 2-(dimethylamino)ethanethiol (DMAET) ligands on the surface cannot be destabilized using this strategy. CdSe/CdS(+) NRs grafted with DMAET exhibit a positive charge as the amine of the ligand is protonated in a slightly acidic HCl solution. The particles possess a positive zeta potential and gelation with positively charged ions is inhibited. Therefore, negative multivalent

ions are required to bridge these particles into a network. For this purpose,  $S^{2-}$ -ions from  $Na_2S$  dissolved in water can be introduced to an ethanolic NR solution. The bridging leads to nanoscopically dense structures, where particles are preferentially linked side by side as was reported in our publication.<sup>[30]</sup> The NRs have previously been studied as self-supporting gels. The situation is, of course, different for wire gels, which we have studied separately under these gelling conditions. In the case of  $Yb^{3+}$ , we obtain self-supporting wire networks. With  $S^{2-}$ -ions as the gelling agent, it is not possible to produce self-supporting structures from pure Au wires because the wires have a negative surface charge. To obtain such structures even with  $S^{2-}$ -ions, the surface of the Au nanowires must be modified with DMAET accordingly. In the case of mixing with CdSe/CdS NRs, the Au wires are embedded in the network of the CdSe/CdS NR backbone.

Figure 1A,C shows the difference between the structure of the pure NR gel networks gelled with  $S^{2-}$ -ions (A) and  $Yb^{3+}$ -ions (C). In case of  $S^{2-}$ -ions, the particles arrange dominantly side by side, while  $Yb^{3+}$ -ions lead to mainly tip-to-tip connected building blocks, which appears in a branched network structure. To facilitate the recognizability of the arrangement, Figure S1, Supporting Information, contains an image by transmission electron microscopy (TEM) of a sample site with the corresponding schematic representation of the CdSe/CdS NRs in the network.

In case of mixing the NRs with Au nanowires containing MPA ligands on the surface prior to gelation (see Figure 1B,D; for lower magnification, see Figure S2, Supporting Information),

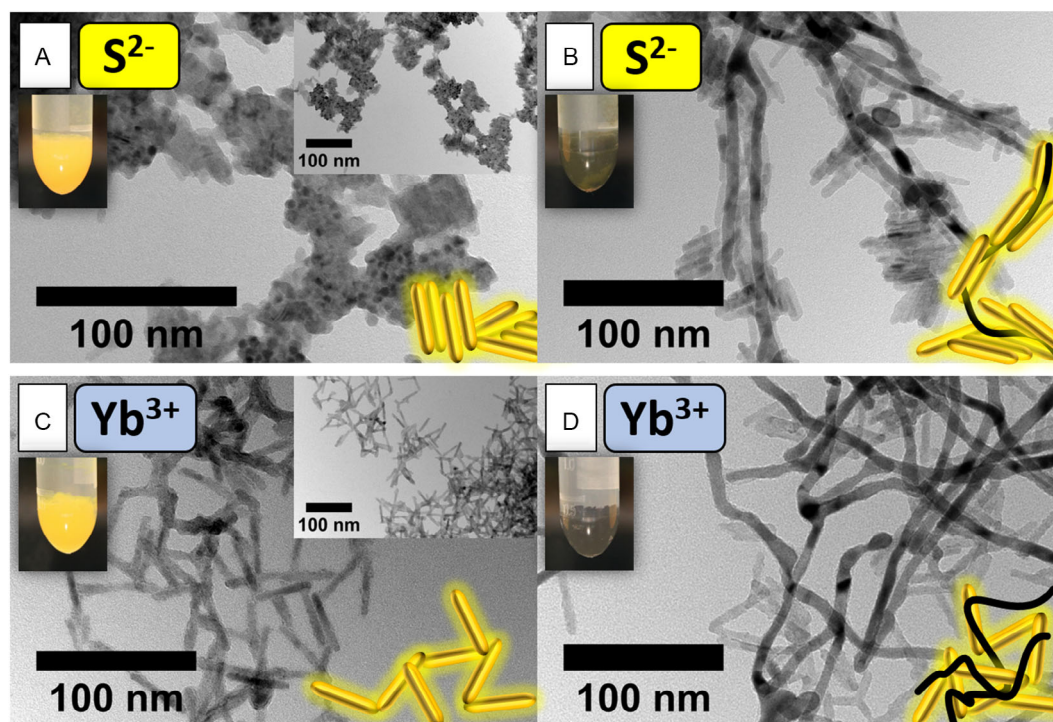


**Figure 1.** Transmission electron microscopy (TEM) captions of hydrogel samples. CdSe/CdS nanorods (NRs) gelled with A)  $S^{2-}$ -ions, and C)  $Yb^{3+}$ -ions (lower magnification inset) and CdSe/CdS:Au-mixed samples with Au nanowires B)  $S^{2-}$ -ions, and D)  $Yb^{3+}$ -ions. Schematics in the lower right corner depict the arrangements. Inset shows pictures of the macroscopic and self-supporting gel networks for each sample.

it can be observed that the Au nanowires are located inside the resulting networks. The Au nanowires and all other components are homogeneously distributed in the overall macroscopic structure which is presented as scanning electron microscopy (SEM)-energy-dispersive X-ray spectroscopy (EDXS) mapping in Supporting Information (see Figure S10, Supporting Information). Closer inspection implies (see Figure S3, Supporting Information, for higher magnification image) a remarkable difference in the interaction of CdSe/CdS NRs and the Au nanowires depending on the gelation route, which also comes from the differences in surface charges of the involved nanomaterials. For  $S^{2-}$ -ion-gelled networks, the Au nanowires are surrounded and covered by the CdSe/CdS(+) semiconductor NRs; thus, the components have a significantly larger contact area in the mixed structure. We assume a pre-coordination of positively charged CdSe/CdS(+) NRs and negatively charged Au nanowires, which result in surface coverage of Au nanowires by CdSe/CdS(+) NRs. Networks obtained by the addition of  $Yb^{3+}$ -ions show a smaller number of contact sites between semiconductor and noble metal due to the branched structure of the semiconductor backbone and the absence of pre-coordination of CdSe/CdS(-) and Au nanowires due to the same charge at the surfaces. This suggests a significantly different network formation mechanism:  $Yb^{3+}$ -ions initiate a rapid built-up of the tip-to-tip connected network which coexists with the Au nanowires. However, a much larger fraction

of NRs destabilized with  $S^{2-}$ -ions align around heterogeneously on the nanowire network. All types of nanomaterial networks appear with very rough surfaces as seen in SEM pictures, see Figure S10, Supporting Information, for  $Na_2S$  and Figure S11, Supporting Information,  $YbCl_3$  system.

To investigate the photoelectrochemical properties of the interpenetrated network structures with Au nanowires, linear sweep voltammetry (LSV), intensity-modulated photocurrent spectroscopy (IMPS), as well as electrochemical impedance spectroscopy (see Figure S4, Supporting Information) were performed. A 0.5 M  $Na_2SO_3$  was used as a hole scavenger during all measurements. **Figure 2** shows the LSV measurements of the pure and the mixed networks. Figure 2A,B includes the pure CdSe/CdS networks (red line) in addition to the interpenetrated gels with Au for ease the comparison of the different networks. Detailed investigation in monolayered CdSe/CdS single crystals can be seen in our recent publication.<sup>[32]</sup> The dark current (which was measured in the time periods when the light emitting diode (LED) was turned off) is about two orders of magnitude higher in the mixed samples (black curves in 2A and B) than in the pure CdSe/CdS samples. Also the increase of the current shows a steeper trend. This observation is in line with expectations, as the Au nanowires exhibit high conductivity. The blue areas in the graph show the samples with light irradiation at 470 nm in each case. The difference of the measured currents between irradiation and darkness reflects the value of the photocurrent.

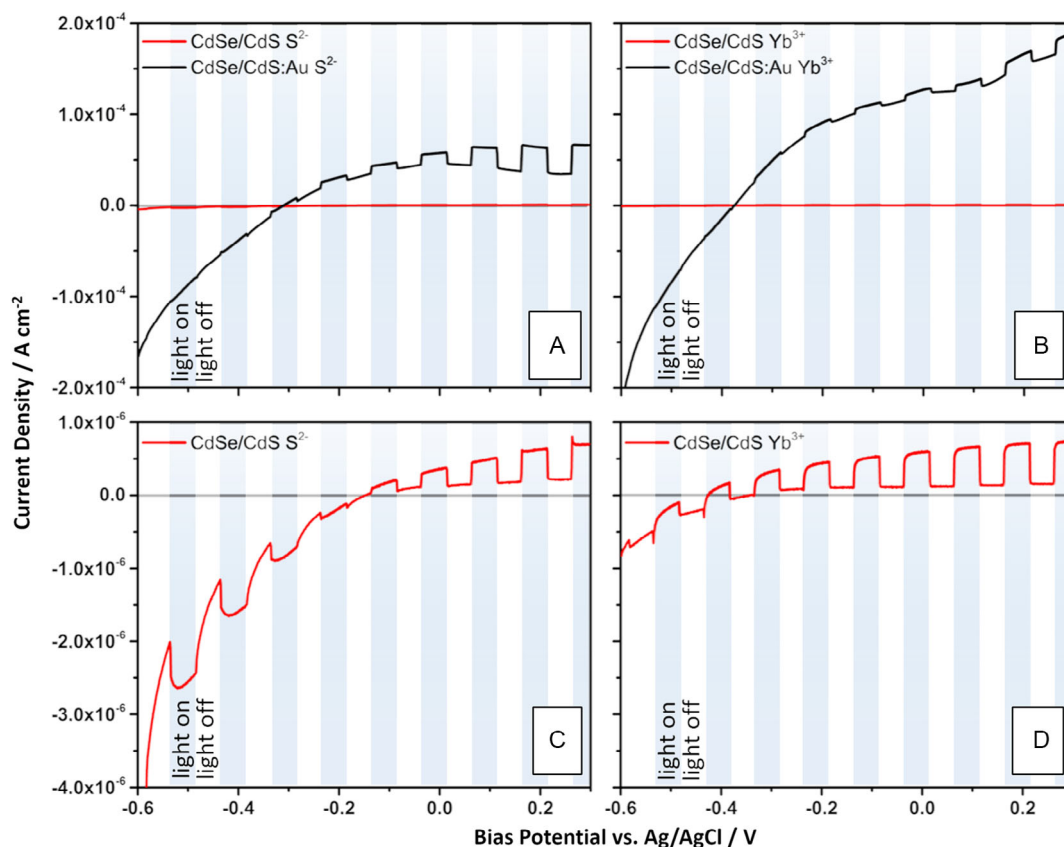


**Figure 2.** Linear sweep voltammetry (LSV) measurements of hydrogels. Hydrogels from A,C)  $S^{2-}$ -ions and B,D) from  $Yb^{3+}$ -ions. Red line in (A,B) corresponds to the pure semiconductor network for the comparison of the highly different absolute values.

It can be clearly seen here that the samples with Au nanowires provide a photocurrent that is two orders of magnitude larger than without Au nanowires. Excited electrons in the semiconductor can be transferred efficiently to the Au nanowires due to the Fermi level of the gold laying in between the bandgap of the semiconductor. The high conductivity of the Au nanowires then enables the transport of the electrons to the electrode to contribute to the measured photocurrent. In the pure semiconductor networks, excited electrons can be transferred through the network toward the electrode. However, the conductivity is much lower which leads to a smaller measured photocurrent. The comparison of both gelation methods shows that the  $S^{2-}$ -gelled system with Au has higher positive photocurrents than the network gelled with  $Yb^{3+}$ . This effect highlights the difference in the contact between gold nanowire and CdSe/CdS semiconductor, which is (based on the TEM images) better in the case of  $S^{2-}$  gelation. The electrons, which are excited upon irradiation, can more easily be transferred to the Au nanowire and further toward the electrode. The pure semiconductor gels show very low dark current. The photocurrent is minimally higher in the network with  $Yb^{3+}$ -ions. The reasons for this are not yet conclusively understood, however, the structural differences can be the subsequent changes of the optical properties (charge-carrier dynamics) certainly play an important role. One possible reason could be explained on the basis of trap states. The introduction of  $S^{2-}$ -ions<sup>[30]</sup> for gelation generates additional sulfur bonds. These sulfur bonds can present trap states for holes,<sup>[33]</sup> reducing

the photocurrent. Furthermore, charge transfer can also occur within the network generated by  $Yb^{3+}$  to the electrode, as recently discussed in our previous publication.<sup>[31]</sup> Since the CdSe/CdS particles are preferentially arranged tip to tip, there are smaller contact areas where the electrons may react with defects, thus not further reducing the photocurrent generation.

To get insight into the dynamics of the charge-carrier transfer, IMPS measurements were conducted on the gel networks shown in **Figure 3**. This type of measurement visualizes the contribution of the different charge-transfer pathways. In the case of all samples, it can be seen that the measured values result in two semicircles. The first semicircle is partly faint (3A–C) and locates around the origin representing the short charge-transfer paths near the electrode. Samples that do not contain Au nanowires show only a small second semicircle. This demonstrates that the contribution of nanoparticle-electrode transfer overcomes the transport in the network itself. In general, the charge-carrier transport in networks, which is attributed to the second semicircle,<sup>[34]</sup> containing  $Yb^{3+}$ -ions is more pronounced than in those prepared using  $S^{2-}$ -ions. When the samples contain Au nanowires, much more pronounced second semicircle evolves in the case of the  $S^{2-}$ -gelled networks (the real part of the external photocurrent quantum efficiency is a factor of five larger than in the  $Yb^{3+}$  network). This observation is in line with the structural nature of the mixed samples, in which the semiconductor–metal contact in the case of the  $S^{2-}$ -gelled networks is more prominent. It can be assumed that the charge

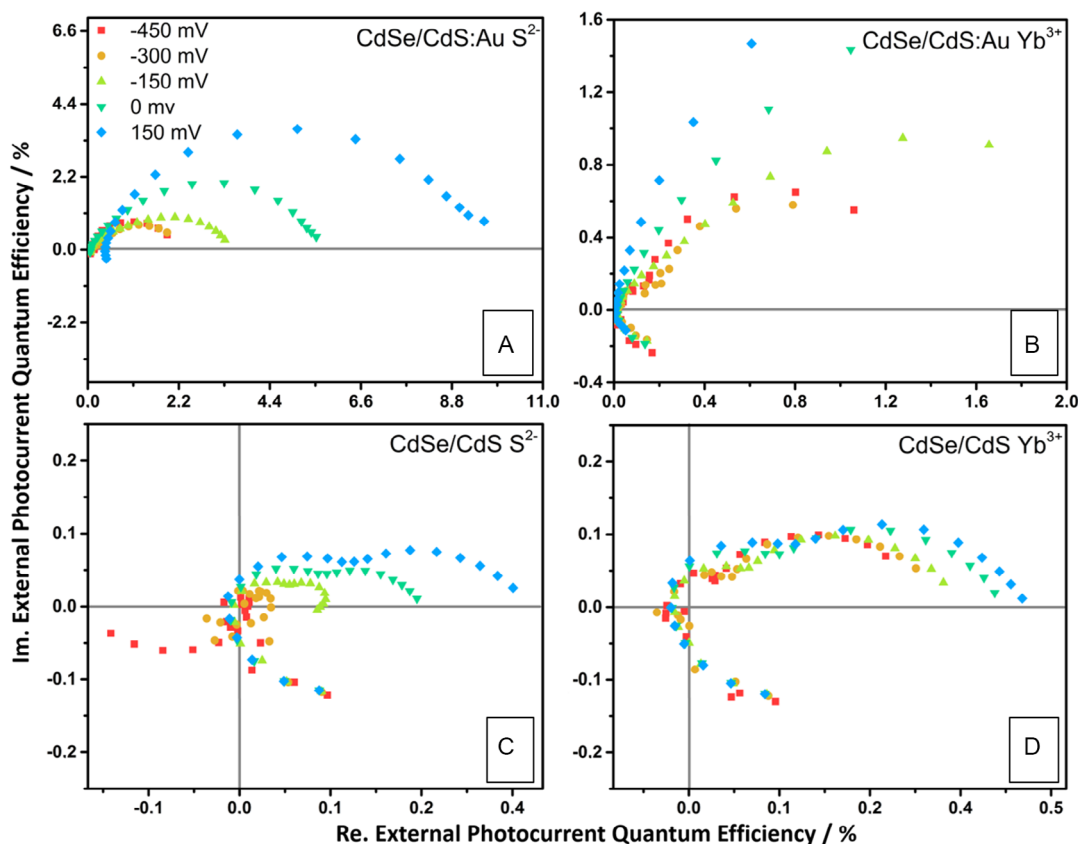


**Figure 3.** Intensity-modulated photocurrent spectroscopy (IMPS) Nyquist plots of hydrogels. Hydrogels from A,C)  $S^{2-}$ -ions and B,D) from  $Yb^{3+}$ -ions.

transport occurs primarily through the Au nanowires, which are better integrated into the network upon using  $S^{2-}$  ions. The photocurrent quantum efficiency is an order of magnitude higher (and thus the highest among the investigated samples) in the case of the  $S^{2-}$  networks than in  $Yb^{3+}$  networks. This emphasizes the importance of the nanostructuring of multicomponent gel networks, where the effect of the contact between the different materials can dominate the photophysical properties of the macrostructure. As we experienced, the photoelectrochemical measurements are very sensitive with respect to electrolyte, pH, amount of sample, light intensity, and temperature. A comparison of absolute values for different systems is quite inaccurate. However, for hybrid CdSe/CdS/Au-decorated particles, it has been shown that the domain size and distribution of the noble metal affects the charge-carrier separation in these systems, which is most effective for CdSe/CdS NRs tipped with Au.<sup>[35]</sup>

In summary, the electrochemical measurements support the findings deduced from the structural differences seen in the TEM images. It is important to emphasize that the integration of the Au nanowires into the semiconductor NR network succeeded and the photoexcited charges are able to be transferred from the CdSe/CdS NRs into the Au nanowire network. As expected, the conductivity is highly improved by the fact that the networks contain conductive Au nanowires. Connecting CdSe/CdS using different ions results in differences of the contact between semiconductor and metal and hence in a different photoelectrochemical behavior of the nanosystems. Due to the strong bonding of the semiconductors to the Au nanowires in samples gelled by means of  $S^{2-}$  ions, the charge carriers generated by photon excitation can travel toward the electrode supported by the gold network.

### 3. Conclusion

It has been shown that by choosing the appropriate gelling agent, an interpenetrating structure of semiconductor nanoparticles and noble metal nanowires can be obtained, which enables effective charge-carrier separation.  $Yb^{3+}$  cations induce a network formation having branched structure and lower interparticle contact areas. However, a more robust bonding of the semiconductor to the noble metal works can be achieved in the case of the networks gelled with  $S^{2-}$  ions. Here, the photoelectrochemical measurements showed that an effective charge-carrier transport from the semiconductor to the Au nanowires takes place. It can be concluded that the presence of a conductive Au nanowire backbone in the multicomponent structures enables the extensive extraction of photoexcited electrons resulting in significantly higher photocurrents upon illumination than in state-of-the-art nanocrystal gels. We observe two orders of magnitude higher photocurrent in samples containing Au nanowires compared to pure CdSe/CdS NRs samples. Recently, we have prepared various gel structures which were characterized by spectroelectrochemistry and found that the mobility of the photoexcited carriers can be significantly improved via assembling the building blocks into gel networks.<sup>[20,31,32,34,36]</sup> Nevertheless, the photoelectrochemical investigations of the present structures can be further extended by introducing

additional scavengers to the electrolyte solutions, which might help reveal the effect of surface attached ions as well. Future work on the topic of interpenetrated nanoparticle networks could address theoretical calculations involving charge-carrier transport at the interfaces between semiconductors and nanowires. For two connected CdSe/CdS, theoretical calculations have been done for electron and hole.<sup>[21]</sup> Furthermore, charge-carrier transport within the network is also of great interest, where again theoretical calculations may be a supporting tool.

### 4. Experimental Section

**Chemicals:** Tri-*n*-octylphosphine oxide (TOPO, 99%), sulfur (S, 99.98%),  $\alpha$ -naphthol (99%), 1-octadecene (ODE, 90%), chloroform (CHCl<sub>3</sub>, 99.8%), (3-mercaptopropyl)trimethoxysilane (MPTMS, 95%), hydrogen peroxide H<sub>2</sub>O<sub>2</sub> (35%), ammonium hydroxide solution (NH<sub>4</sub>OH, 28–30%), and MPA (99%) were purchased from Sigma Aldrich. Tri-*n*-octylphosphine (TOP, 97%) and potassium hydroxide (KOH, 85%) were purchased from ABCR. Cadmium oxide (CdO), hydrogen tetrachloroaurate(III) trihydrate (HAuCl<sub>4</sub> · 3H<sub>2</sub>O, 99.99%) and selenium (Se, 99.99%) were purchased from Alfa Aesar. Hexylphosphonic acid (HPA, 99%) and octadecylphosphonic acid (ODPA, 99%) were purchased from PCI Synthesis. DMAET hydrochloride (95%) is purchased from Acros. All chemicals were used as purchased and without further purification. Substrates for electrochemical measurements were indium tin oxide (ITO) glass with a height of 1.1 mm coated unpolished soda lime float glass, VisionTek, 12  $\Omega$  sq<sup>-1</sup>.

**Synthesis of CdSe Seeds:** The synthesis of CdSe seeds is according to Carbone et al.<sup>[37]</sup> In this synthesis, CdO (0.06 g, 0.47 mmol), ODPA (0.28 g, 0.84 mmol), and TOPO (3.0 g, 7.76 mmol) were mixed in a 25 mL flask in vacuum and heated to 150 °C. After 1 h, vacuum was switched to argon while the flask was heated to 300 °C for dissolving the CdO until a clear solution was obtained. TOP (1.8 mL, 4.04 mmol) were added to the solution and the flask was heated to 380 °C. At this temperature, a mixture of TOP (1.8 mL, 4.04 mmol) and Se (0.058 g, 0.73 mmol) was injected in the flask quickly.

With 4 mL quickly injection of ODE, the reaction was quenched after 4 min and the heating mantle was removed. When the flask was cooled down to 90 °C, toluene (5 mL) was added into the flask. The particles were precipitated with methanol (8 mL) and redissolved in hexane (8 mL) for purification. This step was repeated twice, and the particles were finally stored in hexane (2 mL).

**CdSe/CdS Dot-in-Rod Particles:** This synthesis was carried out by a seeded-growth method.<sup>[37]</sup> CdO (0.06 g, 0.47 mmol), HPA (0.08 g, 0.48 mmol), ODPA (0.28 g, 0.84 mmol), and TOPO (9 g, 23.28 mmol) were mixed in a flask and heated up to 150 °C for 1 h in vacuum. After degassing the atmosphere was switched to argon and the reaction solution was heated to 300 °C until a clear solution was obtained. TOP (1.8 mL, 4.04 mmol) was injected in the flask and the synthesis solution was heated to 350 °C. The prepared spherical CdSe nanoparticles (0.08  $\mu$ mol) in hexane were dried with air flow and redissolved in a TOP:S mixture (1.8 mL, 4.04 mmol TOP and 0.13 g, 4.05 mmol S) in inert atmosphere. This mixture was quickly injected at 350 °C into the aforementioned flask by which the temperature decreased to 285 °C under inert atmosphere. The temperature was held for 8 min after injection and recovered 350 °C. Then, the solution was air-cooled to reach 90 °C at which toluene (5 mL) was injected.

The purification was carried out by alternating precipitation with methanol (4 mL), centrifugation at 3773 rcf and redispersion in toluene (4 mL) for at least three times. The final NR solution was stored in toluene (12 mL). The size of the NRs was measured by TEM from organic solution (preferably from chloroform).

**Phase Transfer of CdSe/CdS NRs with MPA:** The CdSe/CdS NRs in organic solution were transferred into aqueous solution by ligand exchange.<sup>[38,39]</sup> For phase transfer, 6 mL of the nanoparticle solution was precipitated in a mixture of methanol (50 mL), MPA

(1.3 mL, 14.91 mmol) and KOH (0.57 g, 10.16 mmol) and shaken for 2 h at room temperature in centrifugation vials.

After centrifugation (10 min, 8500 rcf), the precipitate was redispersed in 0.1 M aqueous KOH solution (15 mL). The solution was mixed with 1 mL of chloroform and well shaken. After additional centrifugation (5 min, 8500 rcf), the upper part containing the clean CdSe/CdS NRs was carefully transferred to a new vial. The concentration was determined by atom absorption spectroscopic (AAS) measurements.

**Phase Transfer of CdSe/CdS NRs with DMAET:** Ligand exchange to DMAET according to Kodanek et al.<sup>[39]</sup> with little modifications was done with 6 mL of the as-prepared CdSe/CdS NRs. CdSe/CdS NRs were precipitated with 6 mL MeOH, centrifuged (10 min, 3773 rcf) and redispersed in 6 mL HCl<sub>3</sub>. The 4.8 mL MeOH and 425 mg DMAET · HCl were added, before 2.4 mL H<sub>2</sub>O was added to the solution. The mixture was shaken for 30 min until all particles were obtained in the aqueous phase. The solution was centrifuged for 10 min at 3773 rcf. The particles were redispersed in 4.8 mL in a slight HCl-acidic aqueous solution at pH 5. The concentration was determined by ASS measurements.

**Synthesis of Au Nanowires:** Au nanowires were prepared according to Jiang et al.<sup>[40]</sup> And, 4.5 mL of an aqueous 0.05 M HAuCl<sub>4</sub>·3H<sub>2</sub>O solution and 4.5 mL of 0.5 M  $\alpha$ -naphthol ethanolic solution were mixed at 60 °C in a vial placed in a water bath. The solution is mixed by pipettes and is not stirred. After 1 min at 60 °C the solution is centrifuged (5 min at 663 rcf). The solution above the Au nanowires is removed and the Au nanowires were redispersed in 5 mL of EtOH. This purification step was repeated three times.

**Ligand Exchange for Au Nanowires:** To exchange the surface ligands of the Au nanowires to MPA, 1.5 mL of the as-prepared nanowire solution was mixed with 1.6 mL of a ligand solution containing 10 mL MeOH, 210 mg KOH, and 260  $\mu$ L MPA. The solution is shaken for 2 h and centrifuged for 5 min at 663 rcf. The supernatant is removed and the Au nanowires were dissolved in 1 mL 0.1 M KOH aqueous solution.

**Preparation of Lyogels:** Colloidal solutions were gelled with pure CdSe/CdS or mixed with Au nanowires by keeping the Cd concentration constant (3.6 mg mL<sup>-1</sup> in the resulting network) in ethanol (for Na<sub>2</sub>S) or 0.01 M KOH (for YbCl<sub>3</sub>) solution. All volumes and concentrations of the used substances for gelation were given in **Table 1**. Phase-transferred

colloidal CdSe/CdS DMAET NRs were precipitated with acetone (1:1 vol.), centrifuged for 5 min at 8000 rcf and redispersed in ethanol. Samples gelled with YbCl<sub>3</sub> were used as purified after the phase transfer. For the gelation with Na<sub>2</sub>S, a 200 mM solution of Na<sub>2</sub>S in water was prepared. The resulting concentration of S<sup>2-</sup> in the gelation solution was kept at 5 mM. In case of interpenetrating particle networks, 1 mg of Au nanowires ( $c = 7.5 \text{ mg mL}^{-1}$ , 133  $\mu$ L) was set for all samples. After addition of the S<sup>2-</sup> or Yb<sup>3+</sup> solution, samples were well shaken and stored at room temperature for 24 h aging process. The network structures were washed five times with ethanol (Na<sub>2</sub>S) or ultrapure water (YbCl<sub>3</sub>) to reduce byproducts and KOH content. The cleaning process was carried out by exchanging the solution above the formed network. Here, the liquid phase was carefully pipetted off and filled with fresh solvent. The waiting time between two washing steps was about 12–24 h to ensure diffusion of the solvent into the pores of the network.

**Functionalization of ITO Substrates:** According to Miethe et al., ITO substrates (size around 15 × 25 mm) were cleaned and activated with the following procedure. Substrates were rinsed with toluene and placed in special teflon holders which contain a magnetic stirring bar at the bottom in order to move the substrates slightly during the process in a beaker. These substrates were slightly stirred for 8 h in a mixture of 30 mL H<sub>2</sub>O<sub>2</sub> (30%), 30 mL NH<sub>4</sub>OH, and 150 mL ultrapure water at 80 °C. Afterward, the substrates were rinsed with ultrapure water and toluene, and placed in 1 vol% MPTMS solution in toluene (2.1 mL MPTMS and 210 mL toluene) for surface modification of the ITO surface at 60 °C overnight and slightly stirred. The ITO substrates were placed in 50 mL fresh toluene to clean from residual MPTMS and byproducts, and dried to place cylinders as mold for gelation on the surface (see sample preparation for electrochemical measurements).

**Sample Preparation for Electrochemical Measurements:** The samples were prepared as xerogel network structures on MPTMS-functionalized ITO glasses. To obtain xerogels, cut rectangular mold with a height of around 1.5 cm from disposable cuvettes (1 × 1 cm area) were first glued onto the functionalized ITO substrate. Transparent joint silicone was suitable for this purpose. The gelation solution was filled into the cuvette and mixed with the respective initiator (Na<sub>2</sub>S or YbCl<sub>3</sub> solution) and shaken. After the washing procedure described earlier, network structures were dried in room air. This process takes about 1–2 days. The glued-on cuvettes were carefully removed and the ITO substrates were used for the electrochemical measurements. The samples were rehydrated in 0.5 M Na<sub>2</sub>SO<sub>3</sub> solution for 5 h prior to the electrochemical measurement inside the measurement cell. The time for the rehydration was needed to ensure the diffusion of the electrolyte into the porous gel networks. In these conditions, networks remain stable and do not disassemble. We assumed that the drying and aging process was necessary to ensure stability of the nanoparticle samples. After 5 h, the measured photocurrents did not change anymore with longer hydration times so that we assumed that equilibrium was reached. The 0.5 M Na<sub>2</sub>SO<sub>3</sub> solution had a pH of 9 which was adjusted with a 46% sulfuric acid solution.

**TEM:** Fragments of lyogels were dropcasted on carbon-coated copper grids (300 mesh, Quantifoil). An Field Electron and Ion Company (FEI) Tecnai G2 F20 TMP microscope was used to perform the measurements, which was operated at 200 kV accelerating voltage.

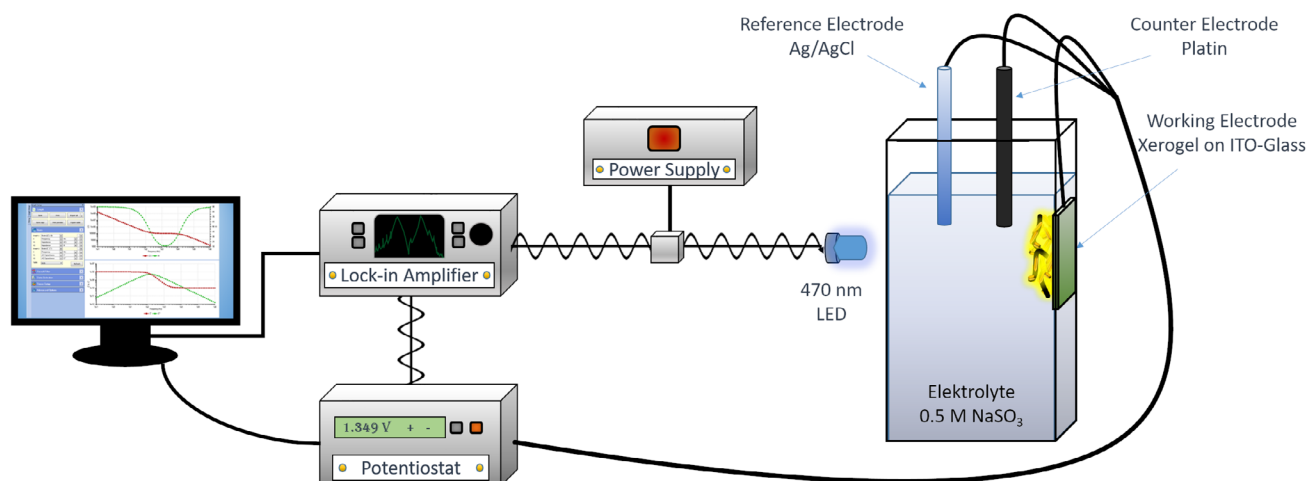
**SEM:** Xerogels were glued on carbon-infiltrated conductive polymer from Plano. SEM images were taken with a JEOL JSM-6700F operated at 2 kV using secondary electron signal and in-lens detector with 3 mm working distance. EDXS mappings were performed with 10 kV accelerating voltage at 15 mm working distance in 25 000 fold magnification and minimum 200 000 signal counts (over 58 frames).

**AAS:** To determine the particle concentrations for CdSe/CdS(+), CdSe/CdS(-), and Au nanowires, AAS spectroscopy was performed with a VARIAN AA140 in acetylene/air flame at element specific wavelength, which was 228.8 nm for Cd and 242.8 nm for Au. Calibration solution concentrations were set to 0, 0.5, 1.0, 1.5, 2.0, and 2.5 mg L<sup>-1</sup> Cd and 0, 5, 10, 15, 20, and 25 mg L<sup>-1</sup> Au. Colloidal nanoparticle solutions were dissolved in aqua regia to obtain ions for the measurement.

**Zeta Potential:** All measurements were performed using a Malvern Zetasizer Nano. To determine the zeta potential values of aqueous

**Table 1.** Overview for lyogel synthesis.

Component	Concentration of initial solution	Volume [ $\mu$ L]	Concentration in the resulting network
CdSe/CdS hydrogels from YbCl <sub>3</sub>			
CdSe/CdS [MPA]	9.3 mg mL <sup>-1</sup>	160.9	3.6 mg mL <sup>-1</sup>
YbCl <sub>3</sub> in H <sub>2</sub> O	50 mM	42	5 mM
H <sub>2</sub> O	–	213.7	–
CdSe/CdS:Au hydrogels from YbCl <sub>3</sub>			
CdSe/CdS [MPA]	9.3 mg mL <sup>-1</sup>	160.9	3.6 mg mL <sup>-1</sup>
YbCl <sub>3</sub> in H <sub>2</sub> O	50 mM	42	5 mM
H <sub>2</sub> O	–	80.7	–
Au wire	7.5 mg mL <sup>-1</sup>	133	2.3 $\mu$ g mL <sup>-1</sup>
CdSe/CdS alcogels from Na <sub>2</sub> S			
CdSe/CdS (DMAET)	8.8 mL <sup>-1</sup>	170.5	3.6 mg mL <sup>-1</sup>
Na <sub>2</sub> S in H <sub>2</sub> O	200 mM	10.5	5 mM
Ethanol	–	235.7	–
CdSe/CdS:Au alcogels from Na <sub>2</sub> S			
CdSe/CdS (DMAET)	8.8 mL <sup>-1</sup>	170.5	3.6 mg mL <sup>-1</sup>
Na <sub>2</sub> S in H <sub>2</sub> O	200 mM	10.5	5 mM
Ethanol	–	102.7	–
Au wire	7.5 mg mL <sup>-1</sup>	133	2.3 $\mu$ g mL <sup>-1</sup>



**Scheme 1.** Schematic setup for (photo)electrochemical measurements. Own graphical representation according to Schlenkrich et al.<sup>[35]</sup>

colloidal solutions, 20  $\mu\text{L}$  of the solution was diluted in 900  $\mu\text{L}$  of the corresponding solution (0.1 M KOH for MPA ligand particles or HCl at pH 5 for particles with DMAET) and then placed in a DTS1070 folded capillary cell. Zeta potential was measured three times for each sample at a temperature of 25  $^{\circ}\text{C}$ . The colloidal solutions remained stable during the measurements without any aggregation. The standard deviation was calculated from the mean value of the three measurements.

*(Photo)Electrochemical Measurements:* **Scheme 1** shows the setup of the measurement used for electrochemical analysis. The sample was placed on a conductive ITO-coated glass and used as the working electrode in the circuit. An electrode with Ag/AgCl (with 3 M NaCl solution) was used as the reference electrode, and platinum served as the counter electrode. The sample was illuminated from the sample side with a 472 nm LED for LSV measurements, and was located in a specially designed teflon cell. During LSV measurements, the photocurrent was measured as a function of the applied potential, which could vary between  $-450$  and  $300$  mV. The measurement was performed at a fixed time interval with a slope of  $4$  mV  $\text{s}^{-1}$ . The LED was periodically turned on and off at a frequency of 40 mHz (corresponding to 12.5 s intervals). In IMPS, electrochemical processes were observed in response to photonic excitation. Sinusoidally modulated light pulses are directed onto the sample, and the frequency of the light was varied for different measurements, which could be set between 10 kHz and 1 Hz using a potentiostat. A lock-in amplifier was required to measure the rapid changes in currents in the nA range. The measurement software used is XM studio ecs 3.4 (Solartron Analytical) for LSV and IMPS measurements. The measurement and frequency modeling were carried out with Acquire Version 4.2.1 (Signal Recovery, part of Ametek Advanced Measurement Technology).

## Supporting Information

Supporting Information is available from the Wiley Online Library or from the author.

## Acknowledgements

The authors thank the German Research Foundation (Deutsche Forschungsgemeinschaft, DFG) under Germany's excellence strategy within the cluster of excellence PhoenixD (EXC 2122, project ID 390833453) and the grant BI 1708/4-3 for funding. R.G. and P.B. are grateful for being funded by the Hannover School for Nanotechnology (HSN). We are thankful for XPS measurements funded by INST 187/789-1. D.Z. acknowledges the project nos. FK-142148 and TKP-2021-NKTA-05

implemented with the support provided by the Ministry of Innovation and Technology of Hungary from the National Research, Development and Innovation Fund, financed under the TKP2021 funding scheme. D.D. would like to acknowledge for the support by the German Research Foundation (DFG research Grant DO 1580/5-1).

Open Access funding enabled and organized by Projekt DEAL.

## Conflict of Interest

The authors declare no conflict of interest.

## Data Availability Statement

The data that support the findings of this study are available from the corresponding author upon reasonable request.

## Keywords

interpenetration, ionic gelation, mixing, multicomponent, nanoparticles, noble metals, semiconductors

Received: July 27, 2023

Published online:

- [1] J. Wang, *Anal. Chim. Acta* **2003**, 500, 247.
- [2] J. L. Mohanan, S. L. Brock, *J. Non-Cryst. Solids* **2004**, 350, 1.
- [3] J. L. Mohanan, I. U. Arachchige, S. L. Brock, *Science* **2005**, 307, 397.
- [4] I. U. Arachchige, S. L. Brock, *J. Am. Chem. Soc.* **2007**, 129, 1840.
- [5] S. Sanchez-Paradinas, D. Dorfs, S. Friebe, A. Freytag, A. Wolf, N. C. Bigall, *Adv. Mater.* **2015**, 27, 6152.
- [6] B. Cai, V. Sayevich, N. Gaponik, A. Eychmüller, *Adv. Mater.* **2018**, 30, 1707518.
- [7] K. L. Kelly, E. Coronado, L. L. Zhao, G. C. Schatz, *J. Phys. Chem. B* **2003**, 107, 668.
- [8] A. P. Alivisatos, *Science* **1996**, 271, 933.
- [9] Q. A. Akkerman, Ph.D. Thesis, University Genua **2019**, [https://dx.doi.org/10.15167/akkerman-quinten-adriaan\\_phd2019-03-14](https://dx.doi.org/10.15167/akkerman-quinten-adriaan_phd2019-03-14).
- [10] L. E. Smart, E. A. Moore, *Solid State Chemistry: An Introduction*, 4th ed. **2016**.

- [11] J. Fricke, in *Aerogels* (Ed: J. Fricke), Springer Berlin Heidelberg, Berlin, Heidelberg, **1986**, ISBN 978-3-642-93313-4 pp. 2–19.
- [12] R. D. Gonzalez, T. Lopez, R. Gomez, *Catal. Today* **1997**, *35*, 293.
- [13] N. Hüsing, U. Schubert, *Angew. Chem., Int. Ed.* **1998**, *37*, 22.
- [14] A. C. Pierre, G. M. Pajonk, *Chem. Rev.* **2002**, *102*, 4243.
- [15] X. Luo, A. Morrin, A. J. Killard, M. R. Smyth, *Electroanalysis* **2006**, *18*, 319.
- [16] Q. Yao, S. L. Brock, *Nanotechnology* **2010**, *21*, 115502.
- [17] Z. Yue, F. Lisdat, W. J. Parak, S. G. Hickey, L. Tu, N. Sabir, D. Dorfs, N. C. Bigall, *ACS Appl. Mater. Interfaces* **2013**, *5*, 2800.
- [18] L. Koralá, J. R. Germain, E. Chen, I. R. Pala, D. Li, S. L. Brock, *Inorg. Chem. Front.* **2017**, *4*, 1451.
- [19] D. Wen, A. Eychmüller, *Chem. Commun.* **2017**, *53*, 12608.
- [20] A. Schlosser, L. C. Meyer, F. Lübkeermann, J. F. Miethe, N. C. Bigall, *Phys. Chem. Chem. Phys.* **2019**, *21*, 9002.
- [21] P. Rusch, B. Schremmer, C. Strelow, A. Mews, D. Dorfs, N. C. Bigall, *J. Phys. Chem. Lett.* **2019**, *10*, 7804.
- [22] M. Rosebrock, D. Zámbo, P. Rusch, D. Pluta, F. Steinbach, P. Bessel, A. Schlosser, A. Feldhoff, K. D. J. Hindricks, P. Behrens, D. Dorfs, N. C. Bigall, *Adv. Funct. Mater.* **2021**, *31*, 2101628.
- [23] T. Mokari, E. Rothenberg, I. Popov, R. Costi, U. Banin, *Science* **2004**, *304*, 1787.
- [24] S. K. Gill, P. Brown, L. J. Hope-Weeks, *J. Sol-Gel Sci. Technol.* **2011**, *57*, 68.
- [25] C. Ziegler, A. Wolf, W. Liu, A. K. Herrmann, N. Gaponik, A. Eychmüller, *Angew. Chem., Int. Ed.* **2017**, *56*, 13200.
- [26] D. Liyanage, D. Z. Spera, R. Sarkar, B. P. Troesch, I. U. Arachchige, *Adv. Photonics Res.* **2021**, *2*, 2100084.
- [27] J. Kang, Z. M. Sherman, H. S. N. Crory, D. L. Conrad, M. W. Berry, B. J. Roman, E. V. Anslyn, T. M. Truskett, D. J. Milliron, *J. Chem. Phys.* **2023**, *158*, 024903.
- [28] T. Hendel, V. Lesnyak, L. Kühn, A.-K. Herrmann, N. C. Bigall, L. Borchardt, S. Kaskel, N. Gaponik, A. Eychmüller, *Adv. Funct. Mater.* **2013**, *23*, 1903.
- [29] L. Nahar, R. J. A. Esteves, S. Hafiz, U. Oezguer, I. U. Arachchige, *ACS Nano* **2015**, *9*, 9810.
- [30] M. Rosebrock, R. T. Graf, D. Kranz, H. Christmann, H. Bronner, A. Hannebauer, D. Zámbo, D. Dorfs, N. C. Bigall, Submitted **2023**.
- [31] D. Zámbo, A. Schlosser, P. Rusch, F. Lübkeermann, J. Koch, H. Pfnür, N. C. Bigall, *Small* **2020**, *16*, 1906934.
- [32] J. F. Miethe, F. Lübkeermann, J. Poppe, F. Steinbach, D. Dorfs, N. C. Bigall, *ChemElectroChem* **2018**, *5*, 175.
- [33] M. Micheel, B. Liu, M. Wächtler, *Catalysts* **2020**, *10*, 1143.
- [34] F. Lübkeermann, J. F. Miethe, F. Steinbach, P. Rusch, A. Schlosser, D. Zámbo, T. Heinemeyer, D. Natke, D. Zok, D. Dorfs, N. C. Bigall, *Small* **2019**, *15*, 1902186.
- [35] J. Schlenkrich, D. Zámbo, A. Schlosser, P. Rusch, N. C. Bigall, *Adv. Opt. Mater.* **2021**, *10*, 2101712.
- [36] A. Schlosser, J. Schlenkrich, D. Zámbo, M. Rosebrock, R. T. Graf, G. Escobar Cano, N. C. Bigall, *Adv. Mater. Interfaces* **2022**, *9*, 2200055.
- [37] L. Carbone, C. Nobile, M. De Giorgi, F. D. Sala, G. Morello, P. Pompa, M. Hytch, E. Snoeck, A. Fiore, I. R. Franchini, M. Nadasan, A. F. Silvestre, L. Chiodo, S. Kudera, R. Cingolani, R. Krahn, L. Manna, *Nano Lett.* **2007**, *7*, 2942.
- [38] H. G. Bagaria, E. T. Ada, M. Shamsuzzoha, D. E. Nikles, D. T. Johnson, *Langmuir* **2006**, *22*, 7732.
- [39] T. Kodanek, H. M. Banbela, S. Naskar, P. Adel, N. C. Bigall, D. Dorfs, *Nanoscale* **2015**, *7*, 19300.
- [40] X. Jiang, X. Qiu, G. Fu, J. Sun, Z. Huang, D. Sun, L. Xu, J. Zhou, Y. Tang, *J. Mater. Chem. A* **2018**, *6*, 17682.